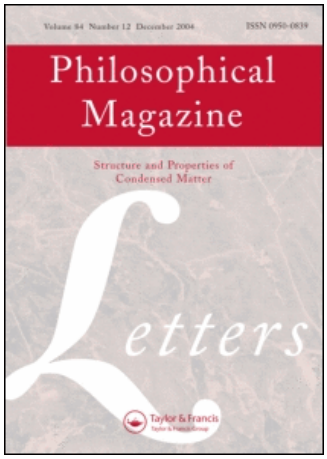

Philosophical Magazine Letters
Publication details, including instructions for authors and subscription information:
http://www.informaworld.com/smpp/title~content=t713695410

Inversion domain boundary in a ZnO film

Y. Z. Liu [a]; H. T. Yuan [a]; Z. Q. Zeng [a]; X. L. Du [a]; X. D. Han [b]; Q. K. Xue [a]; Z. Zhang [b]
[a] Beijing National Laboratory for Condensed Matter Physics, Institute of Physics, Chinese Academy of Sciences, Beijing 100080, China
[b] Beijing University of Technology, Beijing 100022, China

First Published on: 10 July 2007
To cite this Article: Liu, Y. Z., Yuan, H. T., Zeng, Z. Q., Du, X. L., Han, X. D., Xue, Q. K. and Zhang, Z. (2007) 'Inversion domain boundary in a ZnO film', Philosophical Magazine Letters, 87:9, 687 - 693
To link to this article: DOI: 10.1080/09500830701446995
URL: http://dx.doi.org/10.1080/09500830701446995

Philosophical Magazine Letters,
Vol. 87, No. 9, September 2007, 687–693

Inversion domain boundary in a ZnO film

Y. Z. LIU*†, H. T. YUAN†, Z. Q. ZENG†, X. L. DU†,
X. D. HAN‡, Q. K. XUE† and Z. ZHANG‡

†Beijing National Laboratory for Condensed Matter Physics, Institute of Physics,
Chinese Academy of Sciences, P.O. Box 603, Beijing 100080, China
‡Beijing University of Technology, 100 Pingle Yuan,
Chao Yang District, Beijing 100022, China

(*Received 25 November 2006; accepted in revised form 8 May 2007*)

Transmission electron microscopy has been used to investigate the $(\bar{1}100)$ and $(\bar{1}103)$ inversion domain boundaries in a ZnO film prepared by molecular beam epitaxy. The inversion domain was revealed by dark-field images and confirmed by convergent-beam electron diffraction. Interacting with a (0002) stacking fault, the inversion domain boundary in the $(\bar{1}100)$ plane alters its orientation from the [0001] direction and climbs on the $(\bar{1}103)$ plane to release the strain energy. These features are characterized and analysed by high-resolution electron microscopy and the geometric phase method. The findings are significant for understanding the formation and propagation of inverse domain boundaries in epitaxial ZnO films.

1. Introduction

Over the past decades, numerous studies have been focused on the wide-band-gap oxide semiconductor ZnO for its many applications in the electronics industry, particularly in optoelectronics. Its high excitation energy (60 meV) makes ZnO a very promising candidate for laser applications at room temperature [1]. In addition, ZnO is one of the best candidates for a diluted magnetic semiconductor material [2]. However, the prerequisite for such applications is to achieve high quality p- and/or n-type ZnO thin films. There are several different growth techniques to prepare ZnO films with a low defect density. For example, many high-quality epitaxial ZnO thin films have been grown on Al_2O_3 substrates by molecular beam epitaxy (MBE) during the past few years [3]. However, the defects, including rotation domains, dislocations, stacking defaults and inversion domains, cannot be eliminated completely when the growth parameters are not optimized thoroughly. These defects are detrimental to the electronic and mechanical applications of ZnO thin films, for example, via the introduction of electrically active energy levels in the energy gap [4]. It should be emphasized that the inversion domain of III–V and II–VI semiconductors affects impurity incorporation [5] and doping efficiency [6]. ZnO has a similar wurtzite crystalline structure to GaN and they have similar electronic and optical properties.

*Corresponding author. Email: yzliu@blem.ac.cn

Philosophical Magazine Letters
ISSN 0950-0839 print/ISSN 1362-3036 online © 2007 Taylor & Francis
http://www.tandf.co.uk/journals
DOI: 10.1080/09500830701446995

The extended defects in ZnO thin films grown on Al_2O_3 are very similar to the defects that were found in epitaxial GaN thin films grown on the same substrate material [7, 8]. The GaN inversion domain was investigated several years ago, both theoretically [9] and experimentally [10]. However, the ZnO inversion domain boundary (IDB) has only been studied theoretically from a first-principles total-energy calculation [11] and experimental evidence for inversion domains is sparse. In the present work, the classic transmission electron microscope (TEM) dark-field image technique and high-resolution electron microscopy (HREM) have been used to investigate IDBs in ZnO thin films. The geometric phase [12, 13] method was used to visualize the variation of the local displacement field around the IDB area and the correlations of IDB propagation with stacking faults studied experimentally.

2. Experiment and data processing

The ZnO films were grown on α-Al_2O_3 (0001) substrates using radio-frequency plasma-assisted molecular beam epitaxy [3, 4]. Elemental zinc (6 N grade), and magnesium (5 N grade) were used as molecular beam sources in an oxygen plasma (O_2 gas, 6 N grade). The substrates were degreased in trichloroethylene and acetone followed by a deionized water rinse. In order to completely eliminate the formation of rotation domains in the ZnO films, surface modification of the α-Al_2O_3 (0001) substrate was performed using a Mg wetting layer in the growth chamber prior to the growth of the ZnO. The process of modification consists of thermal cleaning of the substrate surface at 750°C, exposure to oxygen plasma for 30 min at 80°C and deposition of a well-defined Mg layer under ultrahigh vacuum at 80°C. Then, the temperature was increased to 300°C, most of the Mg layer was re-vaporized and an ultrathin Mg wetting layer obtained on which the ZnO film growth was begun using a two-step growth method, e.g. a buffer layer growth at 400°C followed by an epilayer growth at 650°C for 3 h. The specimens for TEM investigation were prepared by a standard procedure, which includes mechanical polishing, dimple grinding and low-angle ion milling. The dark-field image and HREM observations were performed with a Philips CM-200-FEG system operated at 200 kV. The NCEM phase extension [14] to Gatan DigitalMicrograph on a Macintosh system were used to process the HREM image in order to find the local lattice displacement near the defect.

3. Results and discussion

The inversion domains in GaN can be characterized by dark-field images [15]. These domains display inversion contrast in TEM dark-field images under $\mathbf{g} = (000\bar{2})$ and $\mathbf{g} = (0002)$ with the electron beam along the non-centrosymmetric $[11\bar{2}0]$ axis. We used the same method to characterize the inversion domain in ZnO. The appropriate dark-field images are shown in figure 1a and b. It is very clear that an inversion domain, marked by the white frame, exists in the middle of the images because this area has reverse contrast in the corresponding two images. As shown in the figures, one is dark while the other is bright. The polarities of the film were

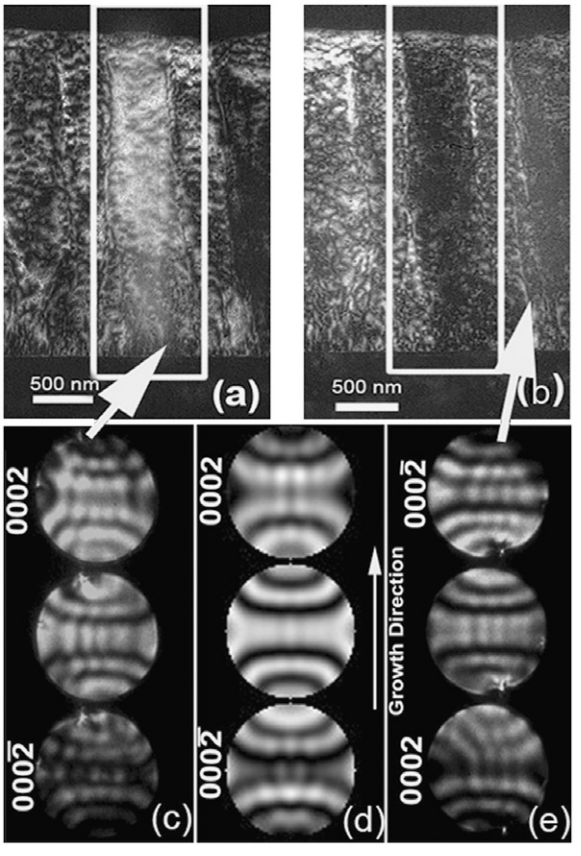

Figure 1. Dark-field TEM images with (a) $\mathbf{g} = (000\bar{2})$ and (b) $\mathbf{g} = (0002)$. CBED patterns for (c) the domain, (d) simulated for a of 140 nm thick Zn-polarity ZnO model with 64 beams included and (e) the remaining areas.

identified by convergent-beam electron diffraction (CBED) by comparing the experimental and Bloch-simulated [16] results, as shown in figure 1c–e. Figure 1c is a CBED pattern taken from the domain region and figure 1e is a CBED pattern taken from another area, as indicated by the large white arrows. Figure 1d is the simulated CBED pattern for a 140 nm thick film of ZnO having Zn-polarity and with 64 beams included. As revealed in figure 1c and 1e, the (0002) and (000$\bar{2}$) diffraction scans exchange black and white contrast. Comparison with the simulated CBED pattern (figure 1d) indicates that the domain has Zn polarity and the remaining areas have O polarity.

In order to picture the IDB clearly, a HREM image was obtained, as shown in figure 2. The IDB lies in the ($\bar{1}$100) plane and is characterized by a white-dot chain as indicated by arrows. It can be interpreted by the model proposed by Yan and Al-Jassim [11]. The grey/white dots represent holes amongst atoms. The dark regions along the grey/white dots in the image are Zn–O atom pairs. The observation direction is along [11$\bar{2}$0]. Across this boundary, the Zn and O positions are

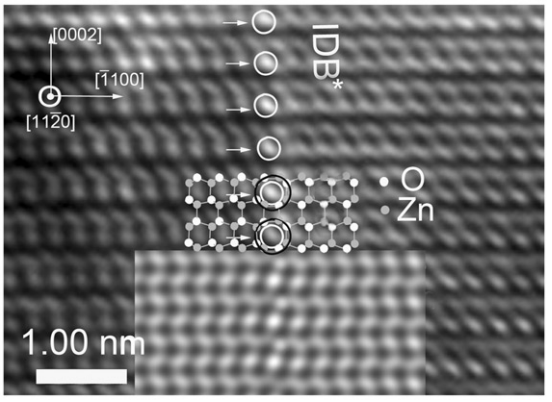

Figure 2. HREM image of the inversion domain boundary taken along the [11$\bar{2}$0] axis. The insert shows the inversion domain model and its HREM simulation.

interchanged, as shown in the insert in figure 2, i.e. the polarity switches across the IDB and the translation symmetry is broken. Based on the previous study [11], the IDB should be bonded by Zn–O atom pairs instead of the unstable ones of Zn–Zn and O–O. Following Yan and Al-Jassim [11], we use IDB* to indicate the Zn–O hetero-atomic bonding structures of the IDB. There are 4(8)-atom chain/channel structures alternately on the IDB*. Although they are energetically favourable and stable, they can trap other interstitial atoms and dopants such as N, C and O [11]. These 8-atom chain/channel structures, which are detrimental, are highlighted by grey circles along the IDB*. They are larger than the regular channels in the ZnO structure. In the HREM image, they appear as bigger white spots, as indicated by the white circles in figure 2. The simulated HREM image based on the IDB* atomic structure model is inserted at the bottom of figure 2. The simulated HREM image agrees well with the experimental one.

The inversion domain boundary is not straight in the dark-field images. We found that part of the IDB* has small distortions. A standard cross-sectional HREM image is shown in figure 3. It reveals that the IDB* is distorted by a stacking fault lying on the (0002) plane, as marked by the white elliptical circle. Interacted with the stacking fault on the (0002) plane, the IDB* alters orientation along ($\bar{1}$100) plane, climbs on the ($\bar{1}$103) and then reverts back to the (0002) plane. The angle between the IDB* glide plane and the (0002) basal plane was measured to be about 31.3° (±5%) which is very similar to the theoretical calculated value of 31.65°, which is the angle between the ($\bar{1}$103) and (0002) planes. As can seen in figure 2 and from Yan and Al-Jassim [11], in order to reduce the boundary energy, the (0001) IDB* consists of a 4(8)-atom Zn–O chain. Interacting with the (0002) stacking fault, the ($\bar{1}$100) IBD* changes orientation to be along ($\bar{1}$103), as shown in figure 3, by the following reaction:

$$(0002)_{\mathrm{StackingFault}} + (\bar{1}100)_{\mathrm{IDB}*} \rightarrow (\bar{1}103)_{\mathrm{IDB}*}.$$

Based on the HREM observations shown in figure 3, this ($\bar{1}$103) IDB* consists of small pieces (steps) along (0002) and ($\bar{1}$100) planes. When the repulsive strain

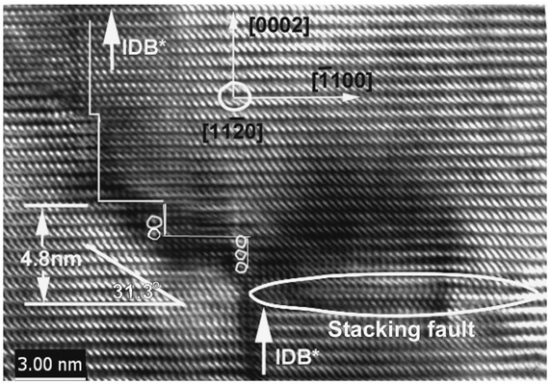

Figure 3. Cross-sectional HREM image of the inversion domain with a stacking fault (from the partial insert layer). The dark contrast near the stacking fault and the glide plane is caused by strain release.

is fully released from the stacking fault region, the ($\bar{1}$103) IDB* will switch back to be along the [0002] direction, as shown in figure 3.

Investigating the elastic and plastic strain fields are important because they are energy favourable sites to trap or nest interstitial or dopant atoms in ZnO films. Studying the contrast in figure 3 carefully, it can be seen that there are strain fields around the stacking fault along the growth direction, i.e. the [0001] direction and the ($\bar{1}$103) IDB*. To picture the strain distribution more efficiently, the geometric phase method was used to map it. This method was used to analyse the lattice variations corresponding to the HREM images. Here we characterize only the displacement field qualitatively. We can characterize the local lattice displacement field by comparing the local lattices with the reference lattice, which was defined by a perfect lattice during data processing. The HREM image of the defective area, as shown in figure 4a, was processed by the NCEM phase extension program embedded in the Gatan DigitalMicrograph software [12, 13]. First, we calculated the fast-Fourier-transformed (FFT) pattern and the power spectrum (PS) of figure 4a. Then the (0002) and ($\bar{1}$100) reflections were masked to perform the inverse Fourier transform (IFT) to obtain the phase image, $P(r) = -2\pi g \partial u(r)$, where $\partial u(r)$ is the displacement field with respect to the lattice planes defined by the frequency $\boldsymbol{g}$. Two non-collinear frequencies, $\boldsymbol{g} = (0002)$ and ($\bar{1}$100), were used to define the reference lattice. The local lattice displacement field along [0001] direction is shown in figure 4b. The elastic/plastic strain field gradient along the [0001] direction has a large impact on the IDB* character. Compared with the perfect lattice, the brighter contrast means a larger displacement field. The dark uniform contrast means the same lattice displacement, indicating a perfect lattice. It reveals that the lattice displacement field shows strong contrast immediately above the stacking fault for the bottom-up grown ZnO thin film.

The strain fields show asymmetrical features on the two sides (up and down) of the stacking fault and this indicates that the stacking fault is a growth defect rather than being introduced by external forces. Both strain fields sitting on the up-side, i.e. along the thin-film growth direction of the defective planes [the (0002) stacking fault and the ($\bar{1}$103) IDB*], confirms that the stacking fault is a growth defect.

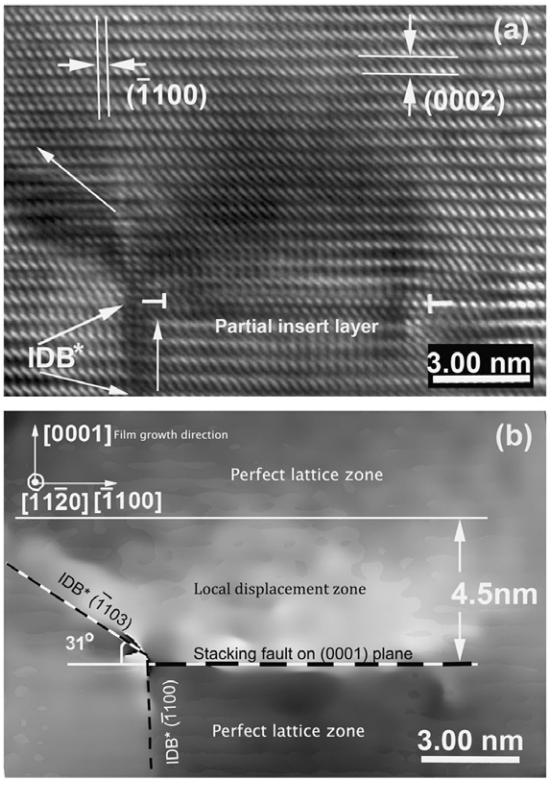

Figure 4. (a) HREM image of the stacking fault and moving IDB*. (b) The local displacement distribution according to the area in (a). The contrast shows the displacement (field) value; brighter means larger displacement. The strain release is clear along the glide plane. It drives the IDB* aside.

Owing to the inserted extra atomic layer on the (0002) plane of the stacking fault, a repulsive elastic strain is created above the stacking fault. The regions below the stacking fault retain the perfect lattice because they were grown prior to the introduction of the stacking fault. All the regions above the stacking fault including the left-side of the $(\bar{1}100)$ IDB* suffer from the strain field in subsequent growth. The direct consequence of the repulsive elastic strain is that the $(\bar{1}100)$ IDB* altered orientation to climb on the $(\bar{1}103)$ plane. The elastic strain field extended to be about 4.5 nm. On releasing the elastic strain field, the lattice relaxes and the $(\bar{1}103)$ IDB* switched back to be along the $(\bar{1}100)$ plane. This is consistent with the HREM result shown in figure 3. We find that the IDB* extending along [0001] again after the stacking fault by about 4.8 nm.

4. Conclusions

In summary, we have identified and characterized the $(\bar{1}100)$ and $(\bar{1}103)$ inversion domain boundaries in an epitaxial ZnO film on a sapphire substrate. Further to the

classic picture of the $(\bar{1}100)$ IDB* in ZnO, we revealed that the $(\bar{1}100)$ IDB* is able to shift orientation with the assistance of elastic strain fields. The geometric phase method was applied to characterize qualitatively the local lattice displacement field near the defect. These finding are useful for understanding and controlling the nucleation and propagation of the IDB* in ZnO thin films.

Acknowledgements

This work was supported by the National Science Foundation (50532090, 60476044) and the Ministry of Science and Technology (2002CB613502) of China.

References

[1] Y. Segawa, A. Ohtomo, M. Kawasaki, *et al*., Phys. Stat. Sol. (b) **202** 669 (1997).
[2] T. Dietl, H. Ohno, F. Matsukura, *et al*., Science **287** 1019 (2000).
[3] Z.X. Mei, X.L. Du, Y. Wang, *et al*., Appl. Phys. Lett. **86** 112111 (2005).
[4] H. Iwata, U. Lindefelt, S. Oberg, *et al*., Phys. Rev. B **65** 033203 (2002).
[5] M. Sumiya, K. Yoshimura, K. Ohtsuka, *et al*., Appl. Phys. Lett. **76** 2098 (2000).
[6] L.K. Li, M.J. Jurkovic, W.I. Wang, *et al*., Appl. Phys. Lett. **76** 1740 (2000).
[7] X.J. Ning, F.R. Chien, P. Pirouz, *et al*., J. Mater. Res. **11** 580 (1996).
[8] D. Gerthsen, D. Litvinov, T. Gruber, *et al*., Appl. Phys. Lett. **81** 3972 (2002).
[9] J.E. Northrup, J. Neugebauer and L.T. Romano, Phys. Rev. Lett. **77** 103 (1996).
[10] G.P. Dimitrakopulos, P. Komninou, J. Kioseoglou, *et al*., Phys. Rev. B **64** 245325 (2001).
[11] Y. Yan and M.M. Al-Jassim, Phys. Rev. B **69** 85204 (2004).
[12] M.J. Hytch, Microsc. Microanalysis Microstruct. **8** 41 (1997).
[13] M.J. Hytch, J.L. Putaux and J.M. Penisson, Nature **423** 270 (2003).
[14] M.H. Roar Kilaas, Phase-extension routines. Available online at: http://ncem.lbl.gov/frames/software.htm(accessed 4 June 2007).
[15] L.T. Romano, J.E. Northrup and M.A. O'Keefe, Appl. Phys. Lett. **69** 2394 (1996).
[16] J.C.H. Spence and J.M. Zuo, *Electron Microdiffraction* (Plenum, New York, 1992).